New examination of the traditional Raman Lidar technique II: evaluating the ratios for water vapor and aerosols - Errata Sheet

David N. Whiteman
NASA/Goddard Space Flight Center
Greenbelt, MD 20771

1 Introduction

This document is intended to correct errors in and expand on Whiteman, David N., "Examination of the traditional Raman lidar technique. II. Evaluating the ratios for water vapor and aerosols", Applied Optics, 42, No. 15, 2593-26 (2003).

2 Corrections to Section 4.B: Aerosol Scattering Ratio - Formulation of the Equations for Aerosol Scattering Ratio

On page 2600, equations 21 - 26 must be revised. The changes below correct the mistaken use of the volume backscatter coefficient instead of the backscatter cross-section. Also, an algebraic error was made in accounting for the ratio of Raman active molecules and the atmospheric number density. The correct equations are listed below.

$$C_N\left(\lambda_L = 351\right) \simeq 0.78 \frac{d\sigma_N\left(\pi\right)/d\Omega\left(\lambda_L = 351\right)}{d\sigma_{mol}\left(\pi\right)/d\Omega\left(\lambda_L = 351\right)} \simeq 0.78 \frac{2.9 \times 10^{-30}}{3.3 \times 10^{-27}} \simeq 6.9 \times 10^{-4} \qquad (21)$$

$$C_N\left(\lambda_L = 355\right) \simeq 0.78 \frac{d\sigma_N\left(\pi\right)/d\Omega\left(\lambda_L = 355\right)}{d\sigma_{mol}\left(\pi\right)/d\Omega\left(\lambda_L = 355\right)} \simeq 0.78 \frac{2.8 \times 10^{-30}}{3.2 \times 10^{-27}} \simeq 6.8 \times 10^{-4} \qquad (22)$$

$$C_N\left(\lambda_L = 532\right) \simeq 0.78 \frac{d\sigma_N\left(\pi\right)/d\Omega\left(\lambda_L = 532\right)}{d\sigma_{mol}\left(\pi\right)/d\Omega\left(\lambda_L = 532\right)} \simeq 0.78 \frac{4.6 \times 10^{-31}}{6.3 \times 10^{-28}} \simeq 5.7 \times 10^{-4} \qquad (23)$$

$$C_O\left(\lambda_L = 351\right) \simeq 0.21 \frac{d\sigma_O\left(\pi\right)/d\Omega\left(\lambda_L = 351\right)}{d\sigma_{mol}\left(\pi\right)/d\Omega\left(\lambda_L = 351\right)} \simeq 0.21 \frac{3.9 \times 10^{-30}}{3.3 \times 10^{-27}} \simeq 2.5 \times 10^{-4} \qquad (24)$$

$$C_O\left(\lambda_L = 355\right) \simeq 0.21 \frac{d\sigma_O\left(\pi\right)/d\Omega\left(\lambda_L = 355\right)}{d\sigma_{mol}\left(\pi\right)/d\Omega\left(\lambda_L = 355\right)} \simeq 0.21 \frac{3.7 \times 10^{-30}}{3.2 \times 10^{-27}} \simeq 2.4 \times 10^{-4} \qquad (25)$$

$$C_O\left(\lambda_L = 532\right) \simeq 0.21 \frac{d\sigma_O\left(\pi\right)/d\Omega\left(\lambda_L = 532\right)}{d\sigma_{mol}\left(\pi\right)/d\Omega\left(\lambda_L = 532\right)} \simeq 0.21 \frac{6.5 \times 10^{-31}}{6.3 \times 10^{-28}} \simeq 2.2 \times 10^{-4} \qquad (26)$$

3 Corrections to Section 4.F.1: Aerosol Scattering Ratio - Atmospheric Calibration of the Aerosol Scattering Ratio - Effect of the Temperature-Sensitivity Functions

The material provided below is intended to completely replace section 4.F.1 of the original paper. This new material corrects errors relating to Fig. 9 and should help clarify the effects of the temperature dependent factors. For reference Eqs. 3, 18, 19, 28 and 29 are repeated here.

$$F_X(T) = \frac{\int_{\Delta\lambda_X} d\sigma_X\left(\lambda^{'},\pi,T\right)/d\Omega\;\xi\left(\lambda^{'}\right)\;d\lambda^{'}}{d\sigma_X\left(\pi\right)/d\Omega\;\xi\left(\lambda_X\right)} \tag{3}$$

$$\frac{P\left(\Delta\lambda_R,r\right)}{P\left(\Delta\lambda_N,r\right)} = \frac{O_R\left(r\right)}{O_N\left(r\right)}\frac{\xi\left(\lambda_L\right)}{\xi\left(\lambda_N\right)}\frac{F_R(T\left(r\right))\beta_\pi^{mol}\left(\lambda_L,r\right)+\beta_\pi^{aer}\left(\lambda_L,r\right)}{F_N(T\left(r\right))N_N\left(r\right)\;d\sigma_N\left(\pi\right)/d\Omega}\Delta\tau\left(\lambda_L,\lambda_N,r\right) \tag{18}$$

$$\beta_\pi^N\left(\lambda_L,r\right) = C_N\;\beta_\pi^{mol}\left(\lambda_L,r\right) \tag{19}$$

$$\mathcal{R}\left(\lambda_L,r\right)-1 = C_N^*\left(\lambda_L,r\right)F_N(T\left(r\right))\frac{P\left(\Delta\lambda_L,r\right)}{P\left(\Delta\lambda_N,r\right)}\Delta\tau\left(\lambda_N,\lambda_L,r\right)-F_R(T\left(r\right)) \tag{28}$$

$$C_N^*\left(\lambda_L,r\right) = C_N\left(\lambda_L\right)\frac{O_N\left(r\right)}{O_R\left(r\right)}\frac{\xi\left(\lambda_N\right)}{\xi\left(\lambda_L\right)} \tag{29}$$

3.1 The Raman Lidar signals and the scattering ratio calculation

Before considering the ways in which the two temperature dependent factors $F_R(T\left(r\right))$ and $F_N(T\left(r\right))$ influence the scattering ratio calculation, a review of the relationship of the Raman lidar signals and the traditional scattering ratio calculation is provided.

Consider the ratio of the Rayleigh-Mie and Raman N_2 signals in Eq. 18 with both of the temperature dependent factors set equal to 1.0. One obtains

$$\frac{P\left(\Delta\lambda_R,r\right)}{P\left(\Delta\lambda_N,r\right)} \propto \frac{\beta_\pi^{mol}\left(\lambda_L,r\right)+\beta_\pi^{aer}\left(\lambda_L,r\right)}{N_N\left(r\right)\;d\sigma_N\left(\pi\right)/d\Omega} \tag{41}$$

Making use of Eq. 19 this can be re-expressed as

$$\frac{P\left(\Delta\lambda_R,r\right)}{P\left(\Delta\lambda_N,r\right)} \propto \frac{\beta_\pi^{mol}\left(\lambda_L,r\right)+\beta_\pi^{aer}\left(\lambda_L,r\right)}{\beta_\pi^{mol}\left(\lambda_L,r\right)} = \mathcal{R} \tag{42}$$

which is the traditional result. Now, for example, when $\beta_\pi^{aer}\left(\lambda_L,r\right)$ = 0, $\mathcal{R}=1$, which is the traditional clear-air normalization condition. When $\beta_\pi^{aer}\left(\lambda_L,r\right)=\beta_\pi^{mol}\left(\lambda_L,r\right)$, $\mathcal{R}=2$; an indication that aerosol and molecular scattering have the same magnitude. In the case of the modified equations that include the temperature dependent factors, the situation is a little more complicated but quite analogous to this.

Consider again Eqs. 18 and 19 but now including the temperature dependent factors. The equation can be expressed as:

$$\frac{P\left(\Delta\lambda_R, r\right)}{P\left(\Delta\lambda_N, r\right)} \quad \propto \quad \frac{F_R(T\left(r\right))\beta_\pi^{mol}\left(\lambda_L, r\right) + \beta_\pi^{aer}\left(\lambda_L, r\right)}{F_N(T\left(r\right))\beta_\pi^{mol}\left(\lambda_L, r\right)} \neq \mathcal{R} \tag{43}$$

where it has been made explicit that this ratio does not now equal the aerosol scattering ratio. When $\beta_\pi^{aer}\left(\lambda_L, r\right)$ = 0, the value of Eq. 43 is $F_R(T\left(r\right))/F_N(T\left(r\right))$, which, as will be shown, becomes the new clear-air normalization value instead of 1.0 as in the case of Eq. 42. Before considering the clear-air normalization procedure, example calculations of $F_R(T\left(r\right))$ and $F_N(T\left(r\right))$ will be given.

3.2 Examples of the temperature dependent factors

Figures 1 and 2 illustrate the calculation of $F_R(T\left(r\right))$ and $F_N(T\left(r\right))$ for the case of 1.5 nm wide Gaussian-shaped passbands that are centered on the Rayleigh and Raman N_2 spectra, respectively. On the left of figure 1, the filter passband is shown along with the pure rotational lines due to molecular N_2 and O_2 that are plotted for temperatures of 180K and 260K. The location of the Cabannes feature is also indicated. On the right is shown $F_R(T\left(r\right))$ as a function of temperature. Its value changes from ~0.982 to 0.987 over the 120K temperature range shown.

The comparable calculations for the Raman N_2 case is shown in figure 2. On the left of figure 2, the filter passband is plotted along with the N_2 rotational-vibrational lines for temperatures of 180K and 260K. The location of the N_2 Q-branch feature is also indicated. On the right is shown $F_N(T\left(r\right))$ as a function of temperature. Its value changes from ~0.895 to 0.915 over the 120K temperature range shown.

3.3 Clear-Air Normalization

The clear-air normalization process entails setting equation 28 equal to 0.0 in a region of the atmosphere that is free of aerosols. This implies that the clear-air normalization condition is

$$C_N^*\left(\lambda_L, r\right)\frac{P\left(\Delta\lambda_L, r\right)}{P\left(\Delta\lambda_N, r\right)}\Delta\tau\left(\lambda_N, \lambda_L, r\right) = \frac{F_R(T\left(r\right))}{F_N(T\left(r\right))} \tag{44}$$

as mentioned above. For the passbands illustrated in figures 1 and 2 and assuming the U.S. Standard Atmosphere temperature profile, the normalization vector $F_R(T\left(r\right))/F_N(T\left(r\right))$ is shown in figure 3. The ratio $F_R(T\left(r\right))/F_N(T\left(r\right))$ varies from approximately 1.08 to 1.09 from the surface to the tropopause.

In general, this ratio is approximately 8% greater than 1.0, which is the value used in the traditional clear-air normalization procedure. It may seem that this implies that, if the temperature dependent factors are ignored, all subsequent calculations will use a molecular value in error by this amount. If $C_N^*\left(\lambda_L, r\right)$ is evaluated from first principles, where, for example, the passband

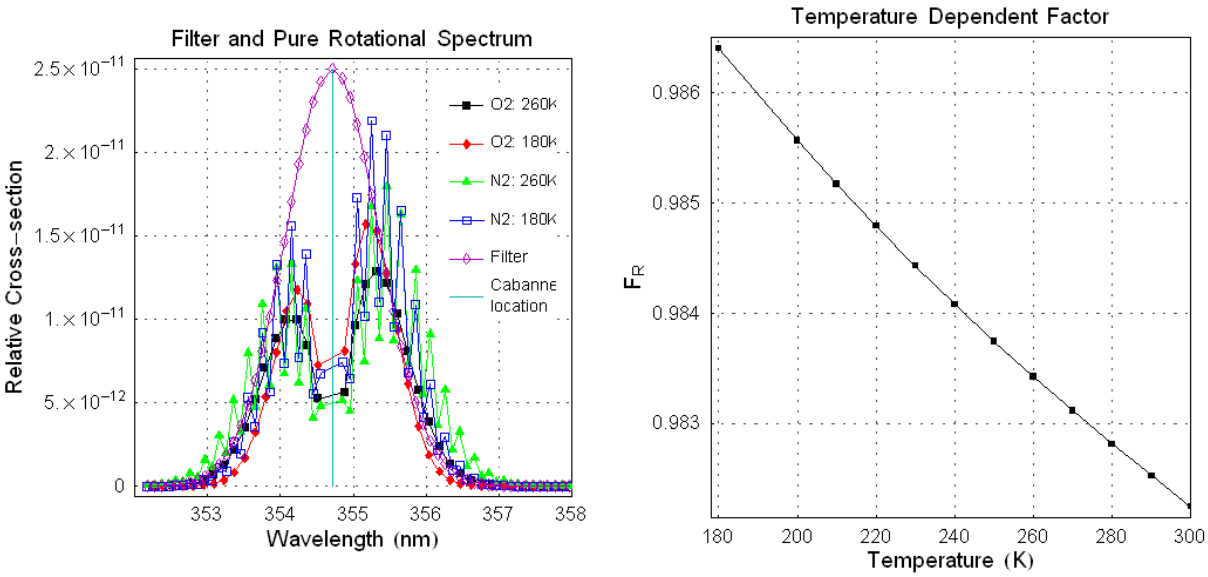

Figure 1: On the left is shown the pure rotational lines N_2 and O_2 at 180 K and 260 K. Also shown in a 1.5 nm Gaussian passband centered on the Cabannes feature. The temperature dependent factor for Rayleigh-Mie channel that results from this passband is shown on the right.

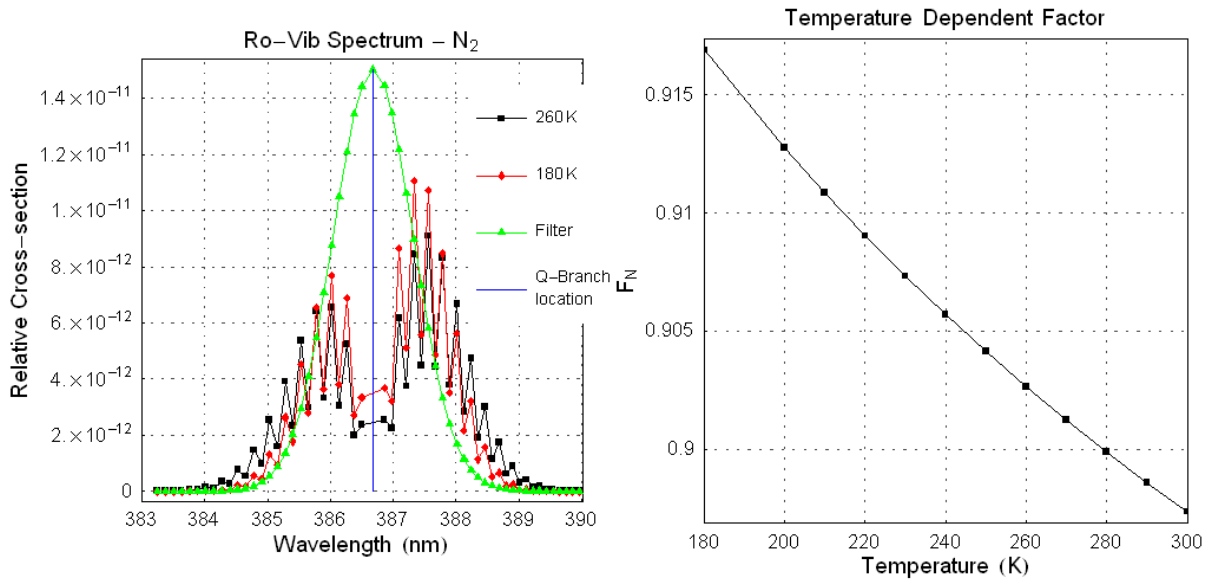

Figure 2: On the left is shown the rotational-vibrational lines of Raman N_2 at 180 K and 260 K. Also shown in a 1.5 nm Gaussian passband centered on the Q-branch. The temperature dependent factor for Raman N_2 that results from this passband is shown on the right.

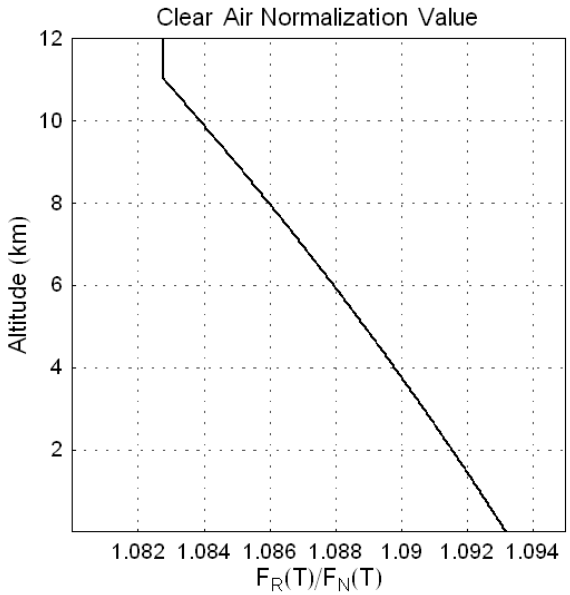

Figure 3: The clear air normalization ratio, $F_R(T(r))/F_N(T(r))$, given in equation 44 plotted as a function of altitude assuming the U.S. Standard Atmosphere.

efficiencies have been determined through spectrally-resolved radiometric measurements, this is indeed the case. However, the typical normalization procedure is to *determine* the value of a normalization constant, one that in general is not equal to $C_N^*(\lambda_L, r)$, through the clear-air normalization process. For the example being considered in figure 3, the normalization value that results will differ from $C_N^*(\lambda_L, r)$ by exactly the ratio shown in the figure to make up for the fact that $F_R(T(r))/F_N(T(r))$ does not equal 1.0. In other words, the clear-air normalization procedure offers compensation for non-unity $F_R(T(r))$ and $F_N(T(r))$. Thus after clear-air normalization, changes in the value of $F_R(T(r))/F_N(T(r))$ between the normalization altitude and some other altitude where the scattering ratio is being caculated change the effective molecular normalization value at this other altitude. The normalization procedure described here accounts for this height-dependent molecular normalization. The separate effects of $F_R(T(r))$ and $F_N(T(r))$ on aerosol scattering ratio calculations are quite different and will now be illustrated using Eqs. 43 and 28.

3.4 The separate effects of $F_R(T(r))$ and $F_N(T(r))$

We will consider the situation where narrow passbands are being used such that $F_R(T(r))$ and $F_N(T(r))$ do not equal 1.0, but where the traditional approach is being followed and these factors are assumed to equal 1.0. In other words, it is assumed that Eq. 43 actually equals $\mathcal{R}$. Consider then that in the numerator of Eq. 43 $\beta_\pi^{aer}(\lambda_L, r)$ must increase from a value of 0 to a value of $F_R(T(r))\beta_\pi^{mol}(\lambda_L, r) < \beta_\pi^{mol}(\lambda_L, r)$ in order for the ratio to double. In the traditional case, a doubling of this ratio would imply $\mathcal{R} = 2.0$. However, in this case, due to the fact that $F_R(T(r))\beta_\pi^{mol}(\lambda_L, r) < \beta_\pi^{mol}(\lambda_L, r)$, a doubling of the value of Eq. 43 indicates that $\mathcal{R} < 2.0$. Thus accounting for the temperature dependent factor $F_R(T(r))$ in the numerator implies that less aerosol scattering is present than the traditional analysis would indicate. The fractional error is independent of aerosol loading and is given by (1- $F_R(T(r))$), which for the 1.5 nm passband illustrated in figure 1 will equal ~1.2% (it can become as large as ~3% for narrower passbands) and varies with altitude due to changes in temperature. The situation is quite similar to that of a High Spectral Resolution Lidar where the rotational Raman lines are excluded[40] from the measurement, and a correction must be made for the excluded part of the cross section. (Given the definition of F_X in Eq. 3 it is actually possible for F_R to exceed 1.0. This can occur for a passband that is centered far from the Cabannes lines so that the transmission of the Cabannes lines is much less than for certain rotational lines. That situation is not considered here. Instead we assume that the passband is centered close to the Cabannes lines so that most of the signal transmitted is due to the Cabannes lines.)

The influence of the term $F_N(T(r))$ on the calculation of $\mathcal{R}$ can be seen most easily from Eq. 28. Here $F_N(T(r))$ directly multiplies the ratio of lidar signals $P(\Delta\lambda_L, r)/P(\Delta\lambda_N, r)$. Since $P(\Delta\lambda_L, r)$ gives the signal from both aerosols and molecules, changes in the value of $F_N(T(r))$ will increase or decrease the apparent signal from both aerosols and molecules. Calculating the aerosol backscatter coefficient from the aerosol scattering ratio (discussed in Section 4.G) requires subtracting the molecular component of the signal from the scattering ratio. If $F_N(T(r))$ is not accounted for in the analysis, increasingly large errors can be made in this subtraction as the amount of aerosols present decreases. The combined effects of the two temperature dependent

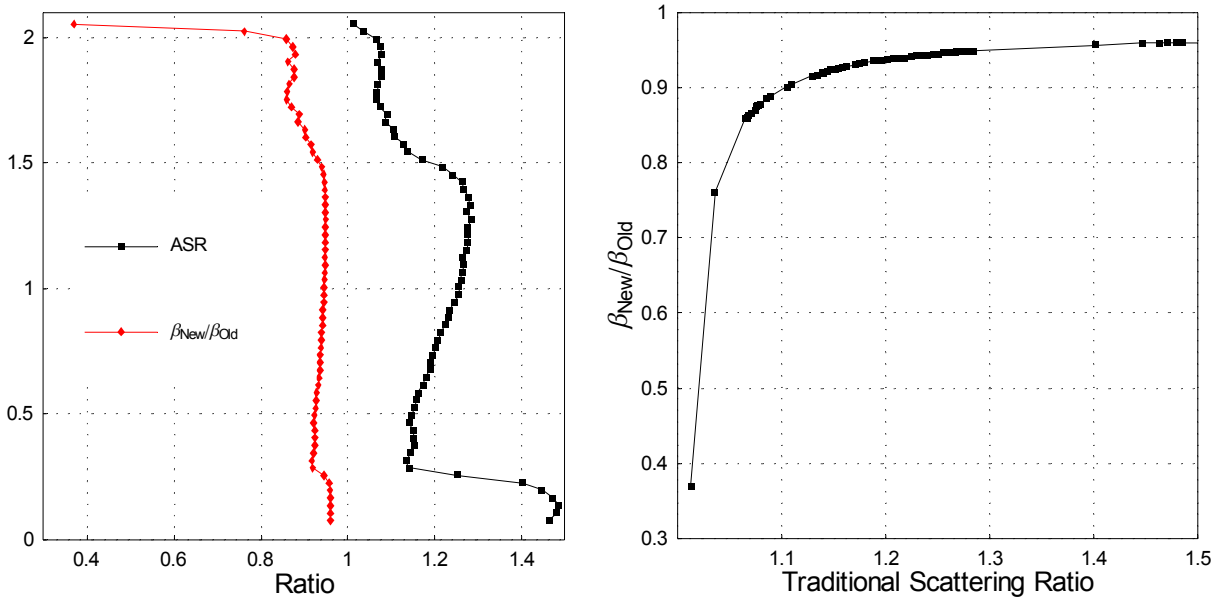

Figure 4: Errors introduced in the calculation of the aerosol backscatter coefficient created by ignoring the temperature-dependent functions is explored here for 1.5 nm-wide Raman nitrogen and Rayleigh-Mie bandpasses. On the left (black) is plotted a one-minute profile of aerosol scattering ratio calculated using the traditional techniques. In red is shown the ratio of new to old aerosol backscatter coefficients where the new analysis takes account of the temperature dependent factors discussed here and the old does not. The data shown in red on the left are reproduced on the right of the figure but this time plotted versus traditional scattering ratio. For this choice of bandpass widths, the error in the quantification of the backscatter coefficient exceeds 10% for all (traditional) scattering ratios less than ~1.1. Ignoring the temperature dependent effects illustrated here will produce values of aerosol backscatter coefficient that are larger than they should be.

factors will now be illustrated with real data.

On the left side of figure 4 and plotted in black is a one-minute profile of aerosol scattering ratio calculated from Scanning Raman Lidar data using the traditional techniques represented by Eqs. 41 and 42 where $F_R(T(r))$ and $F_N(T(r))$ have been assumed to equal 1.0. Plotted in red is the ratio of β_{new}/β_{Old}, where β_{new} is the aerosol backscatter coefficient calculated using $F_R(T(r))$ and $F_N(T(r))$ shown in figures 1 and 2, respectively, and β_{Old} is the aerosol backscatter coefficient calculated using the traditional approach that assumes these factors equal 1.0. For both calculations, a clear-air normalization was performed at approximately 9 km in altitude. The data shown in red on the left are plotted again on the right side of figure 4, but this time as a function of increasing (traditional) aerosol scattering ratio. The curve asymptotically approaches a non-unity value of β_{new}/β_{Old} for increasing traditional scattering ratio. The value of this asymptote is $F_R(T(r))$. For decreasing values of traditional scattering ratio, there is a sharp decrease in the value of β_{new}/β_{Old}. This is the effect of the changes in $F_N(T(r))$ in the denominator of Eq.

43. The value of $F_N(T(r))$ is less in the boundary layer than at the normalization altitude of 9 km implying that the molecular reference has a lower value in the boundary layer. A smaller molecular reference value implies that the same value of the ratio of Eq. 43 will actually imply a smaller amount of aerosols. The error in the aerosol backscatter coefficient increases sharply as the scattering ratio decreases. If the traditional techniques are used, the figure indicates that for a scattering ratio of 1.1 (1.05), the calculated backscatter coefficient will be ~10% (~20%) too small for this combination of passbands. This result implies that previous analyses of narrow spectral band Raman lidar measurements of aerosol backscattering have a positive bias that increases as aerosol loading decreases. The fractional error in the extinction-to-backscatter ratio will essentially be the same.

4 Acknowledgements

Thanks to Volker Freudenthaler and Paolo Di Girolamo for bringing to my attention the algebraic mistakes that have been corrected here.